Modeling of an eye-imaging system for optimizing illumination schemes in an eye-tracked head-mounted display

Hong Hua,[1,*] Craig W. Pansing,[1] and Jannick P. Rolland[2]

[1]3DVIS Laboratory, College of Optical Sciences, University of Arizona, Tucson, Arizona 85721, USA
[2]College of Optics and Photonics, University of Central Florida, Orlando, Florida 32816, USA

*Corresponding author: hhua@optics.arizona.edu

Received 25 April 2007; accepted 31 August 2007;
posted 21 September 2007 (Doc. ID 82403); published 30 October 2007

While the augmentation of head-mounted displays (HMDs) with eye-tracking (ET) capabilities adds challenges to designing compact and portable displays, a systematic approach to integration offers opportunities to improve overall performance and robustness. To investigate the design and optimization of illumination schemes in an ET-HMD system, we present a simulated eye illumination and imaging system, which allows us to explore the critical parameters that affect the quality of the eye illumination. We present details on the modeling process and simulation results. © 2007 Optical Society of America

OCIS codes: 120.2820, 150.2950, 110.3080, 330.2210.

1. Introduction

Both head-mounted displays (HMDs) and eye-tracking (ET) technologies have spawned a wide range of applications in many fields of science and technology [1–4]. Integrating these two stand-alone technologies is highly desirable to create advanced display solutions and instruments to support human factors research [5]. For instance, an eye-tracked HMD (ET-HMD) system can provide a more accurate representation of eyepoint location, which is required by the graphics generation process. An improved eyepoint specification will minimize the perceived angular and depth errors in high-precision displays [6]. Furthermore, such integration can facilitate the creation of more advanced display solutions such as fovea-contingent displays [7].

While some stand-alone HMD and eye-tracker technologies are commercially available, per our experience designing and building HMDs over the last decade we established that their integration from stand-alone technologies, referred to as functionality integration, typically lacks compactness, accuracy, and robustness [8]. We have developed an approach to an integrated ET-HMD instrument where the latter is conceived and optimized as one single instrument from a fundamental design perspective [9–11].

Among the many eye-tracking methods that have been developed [12], a video-based pupil-corneal reflection approach is considered the most practical method to eye tracking in an ET-HMD system [13]. Figure 1 illustrates the schematic of an ET-HMD integration, in which the optical paths for the HMD and eye tracker are combined to share optical elements for minimizing weight and volume. In the eye-tracking path, multiple near infrared emitting diodes (IRED) are mounted around the optics or at locations near the eye to provide illumination. The off-axis IR illumination creates a dark-pupil effect and forms virtual images of the IREDs through the reflection off the anterior cornea. The corneal reflection images are known as the First Purkinje images or glints [14]. The dark pupil, the glints, and the closely surrounding eye-facial structures are then imaged by the optics and captured by an infrared CCD for gaze-direction tracking. Figure 2(a) shows an example of an eye image captured from our testbed system [15,16]. The pupil and glint features move proportionally with eye rotation and differentially between each other [15]. The differential vector between the two

0003-6935/07/317757-14$15.00/0

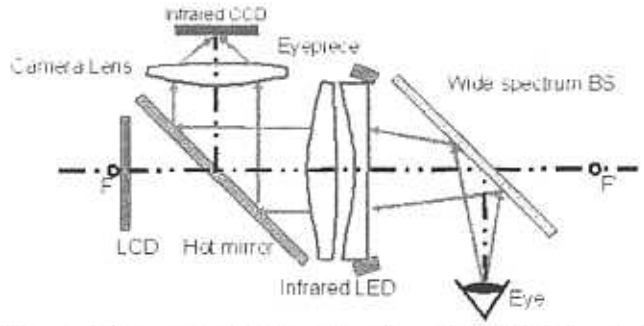

Fig. 1. (Color online) Schematic of an ET-HMD integrated system.

features is used to determine the point of regard of the eye.

Some iris recognition systems aim for security-related applications and require the user to look at a specific target under well-controlled illumination and reduced processing speed requirements. In HMDs, real-time, natural eye movement tracking is required and a critical aspect of the process is thus the quality of the eye illumination under various gaze directions and associated potential spurious reflections. Eye illumination quality plays a critical role in achieving real-time, accurate, and automatic segmentation of the eye pupil and glints from other eye structures and skin surrounding the eyeball. In a well-illuminated eye image, the gray levels of the pupil and glints are well separated from those of other eye-facial structures. Figure 2(b) shows the intensity profile along a horizontal line crossing two of the glints in Fig. 2(a), where the pupil and the glints have the darkest and brightest gray levels. Sufficient contrast was maintained between the darkest pupil and the relatively dark iris and the pupil-iris boundary was well defined. The skin surrounding the eyeball and the sclera were roughly illuminated uniformly with moderate gray levels, thus the high contrast between glints and these relatively bright features was achieved. On the other hand, Fig. 3 shows an ill-illuminated eye image along with its intensity profile along a horizontal scan where discriminability between glints and other structures based on gray level value is more challenging and the gray level of the dark pupil is raised significantly.

Most existing eye-tracking schemes utilize only a single IRED source, and optical illumination software is just starting to provide optimization capabilities. Because of this, to our knowledge, to this date no efforts have been made to develop illumination schemes with a quantitative quality of eye images as a function of one or multiple IRED illumination parameters. The most common practice in controlling the illumination in eye-tracking systems is to manually adjust the illumination sources for a discrete set of test users in a close loop with the testing of the algorithm applied to the images.

The rigid display-tracker platform in an ET-HMD design ensures fixed relationships among the illumination sources, imaging system, display unit, and the eye, and thus offers a unique opportunity to include an optimization of the illumination scheme to yield high-quality eye images that ease the process of feature segmentation. Moreover, we recently demonstrated that geometrical arrangements of multiple sources can be utilized to improve tracking accuracy and extend tracking range [15,16]. The focus of this paper is to explore a simulation-optimization approach to obtaining eye illumination schemes for accurate and robust eye tracking in an integrated ET-HMD.

2. Overview of the Simulation and Optimization Framework

Factors and constraints that affect the eye illumination include the IR source selection and placements as well as human factors such as iris color differences and skin reflectance variations. To systematically analyze these factors for optimal illumination methods in an eye-tracker or ET-HMD system, we propose a simulation-optimization framework based on nonsequential raytracing in which we simulate the elements involved in an eye illumination-imaging system and model several of the necessary human factors by statistical data available from the literature. This approach enables us to include the human factors in the evaluation loop and search for solutions applicable to a population rather than the few individuals who are tested in a laboratory setting. Importantly, the simulated eye images can be analyzed and evaluated through a set of quality criteria driven by the requirements of the image analysis algorithms. The approach can potentially identify illumination schemes that provide optimal tracking accuracy and robustness.

The proposed framework for optimizing eye illumination in an ET-HMD is shown in Fig. 4. It consists of three components: a system modeling module (SMM), an image quality evaluation module (IQEM), and an iterative optimization process (IOP) [17,18]. This section briefly summarizes the functions of the various modules and their relationships in the framework.

A. System Modeling Module

The SMM simulates an eye illumination and imaging system and creates eye images for further quality evaluation. The SMM can be decomposed into three submodules: (1) the illumination scheme characterizer, (2) the illumination generator, and (3) the eye imaging system simulator.

The illumination scheme characterizer defines an illumination method with a radiance distribution generated by a certain IRED configuration on a plane before its incidence on the eye-facial structures. This plane is hereafter referred to as the incidence plane. The radiance distribution on the incidence plane is referred to as the input radiance. Although the incidence plane may be located between the IRED sources and the eye, it was chosen to be a plane tangent to the apex of the cornea for the eye looking straight ahead. The advantage of characterizing eye

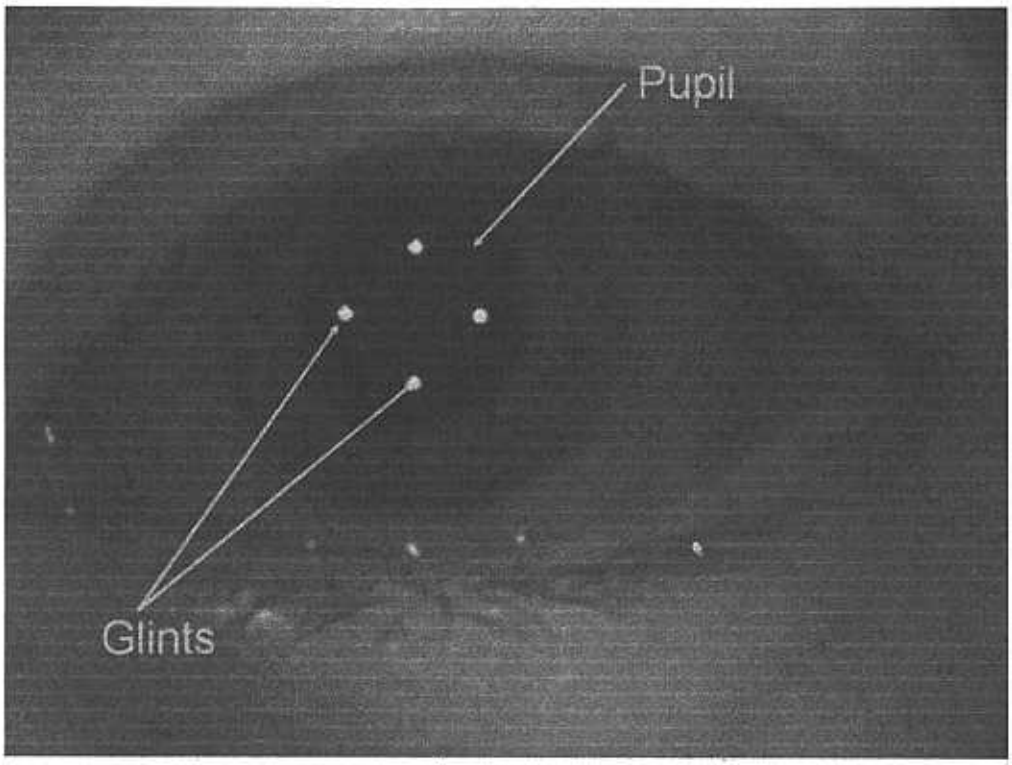

(a)

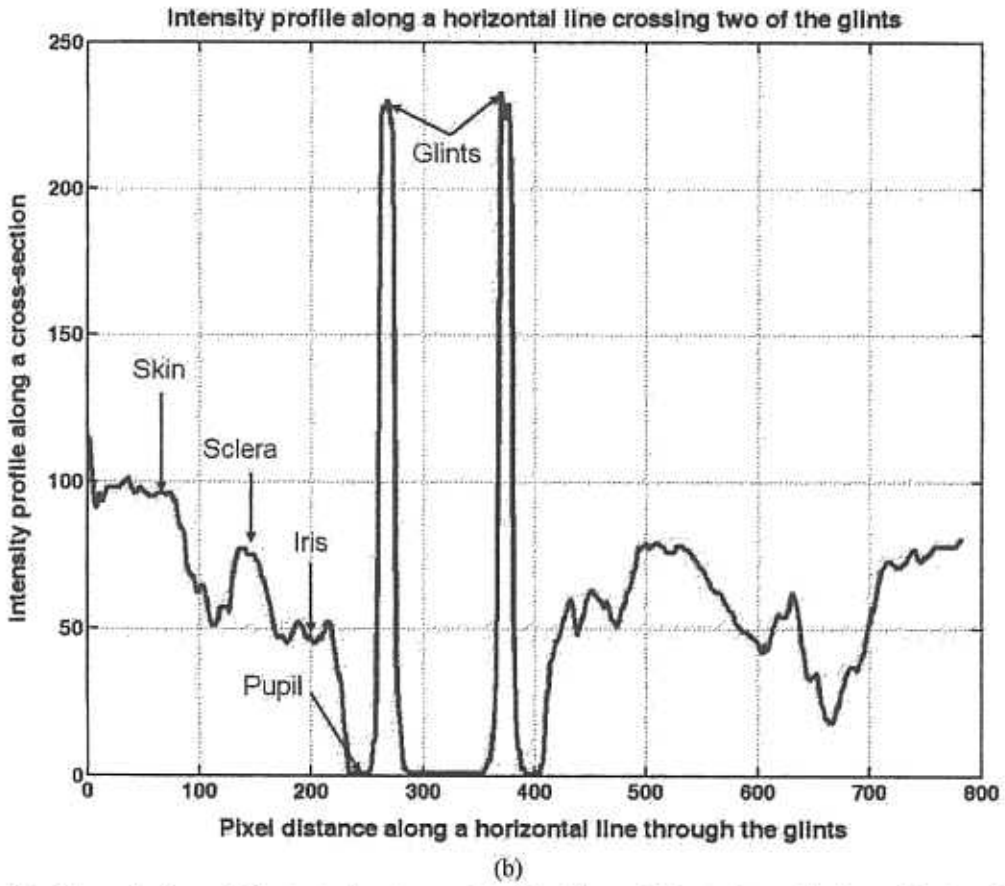

(b)

Fig. 2. (Color online) Example of a well-illuminated eye image: (a) original image; (b) intensity profile along a horizontal line crossing two of the glints.

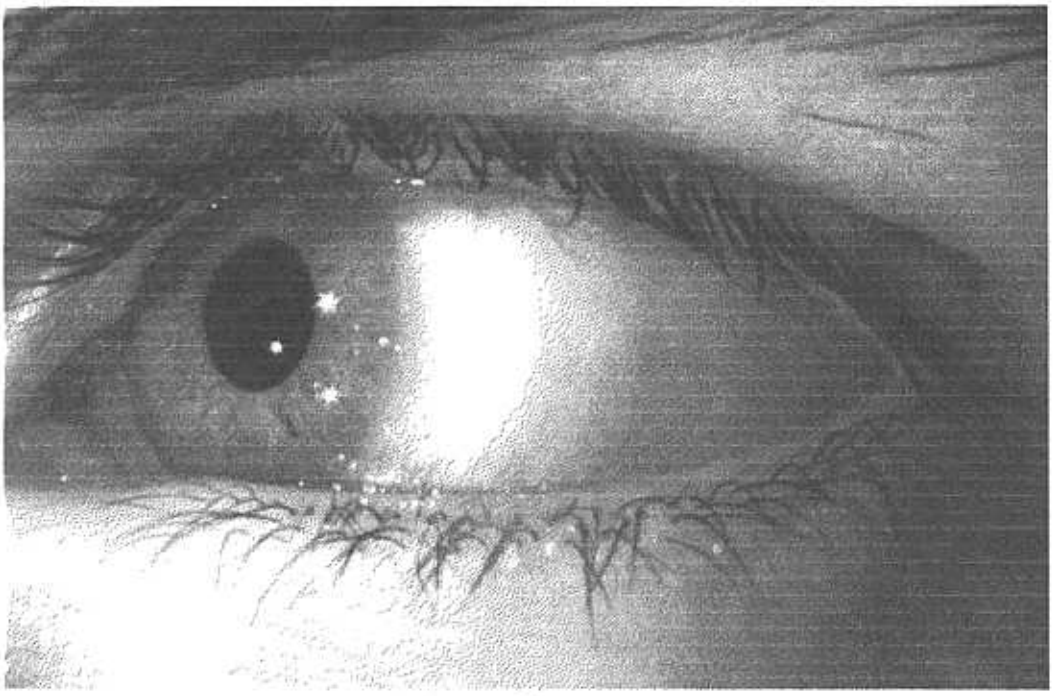

(a)

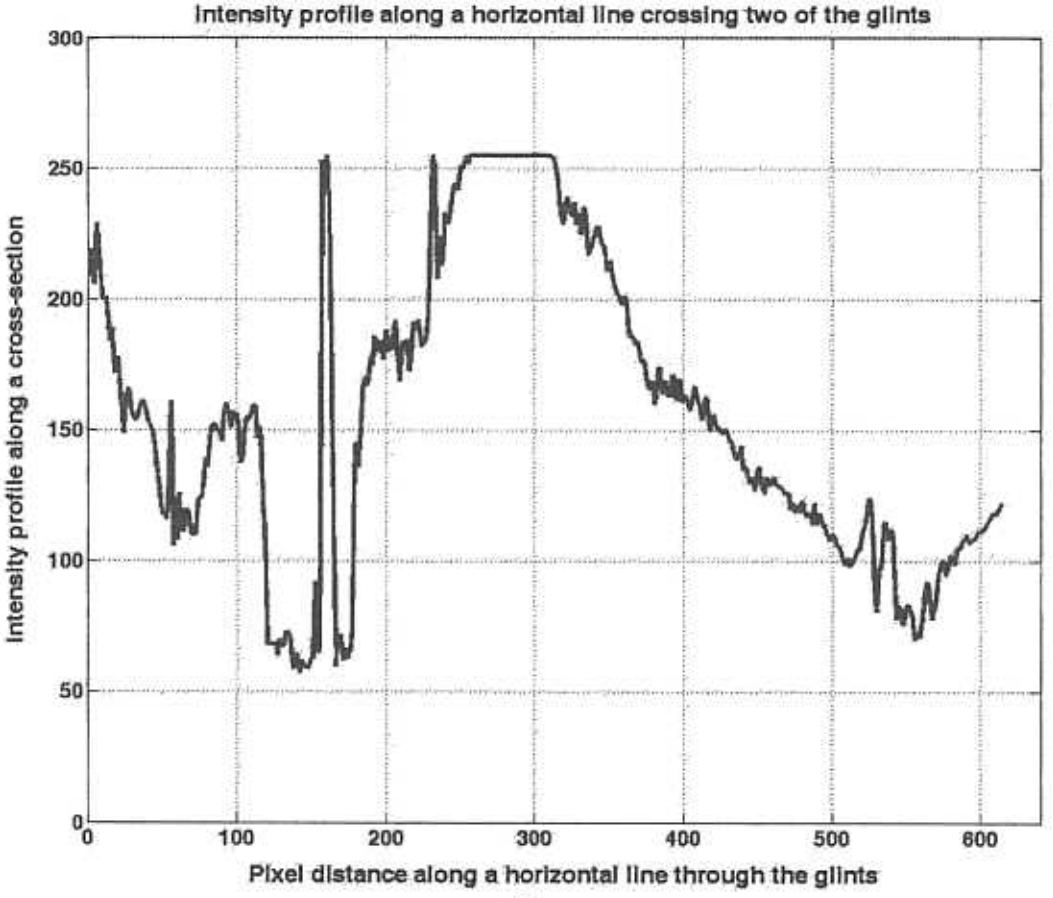

(b)

Fig. 3. (Color online) Example of an ill-illuminated eye image: (a) original image; (b) intensity profile along a horizontal line crossing two glints.

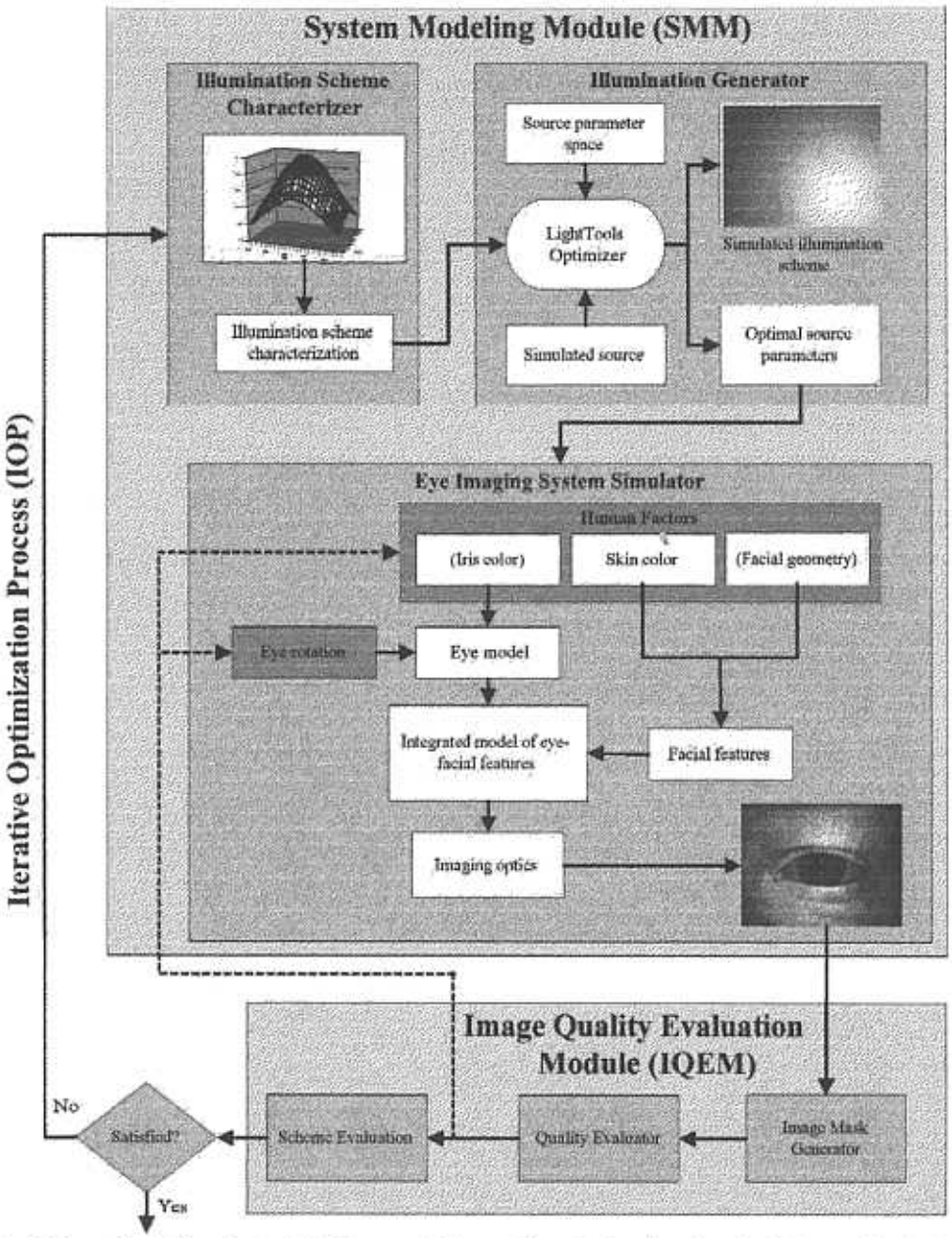

Fig. 4. (Color online) Flow chart of the framework for eye illumination-imaging simulation and optimization.

illumination with the input radiance distribution as opposed to specifying an IRED configuration enables one to decouple the characterization of an illumination scheme from the system-specific parameters and hardware that create such an illumination. An input radiance that is optimized to yield good-quality eye images in one system is applicable to other systems that are designed for the same population and same category of tracking algorithms.

The illumination generator simulates the implementation of an input radiance distribution with real source models and creates the engineering prescription of a given illumination scheme. The generator takes into account specific space and source constraints in an ET-HMD system.

The eye imaging system simulator models the relevant eye and facial structures involved in an eye-tracking system, models the effects of relevant human factors (e.g., iris and skin color variations), and simulates the light interaction between the illumination system and the eye-facial structures. Combining a selected configuration of human factors and a given eye rotation direction, the simulator further simulates an eye image created by an input illumination scheme.

B. Image Quality Evaluation Module

The simulated eye images output by the SMM are input to the image quality evaluation module (IQEM) for feature analysis. While it is beyond the scope of

this paper to discuss the specific quality criteria for the evaluation of image features, the IQEM is introduced here to present a comprehensive description of the overall optimization framework. The function of the IQEM is to define a set of quality criteria driven by the algorithms developed for eye image analysis [15,16] and assesses the quality of a simulated eye image. The IQEM is composed of three submodules: (1) the image mask generator, (2) the quality evaluator, and (3) the scheme evaluator.

The image mask generator creates a set of image masks that represent key features of interest in an eye image. The selection of masks can be customized to the requirements of a particular eye-tracking algorithm. A few mask examples will be given later in Section 6.

The quality evaluator compares an input eye image with its corresponding image masks and segments out individually the key features of interest from the entire image. It then estimates quality criteria that may include the brightness, uniformity, and contrast of these features and the quantitative measurements that provide an indication of the input image quality for tracking.

The loop of eye image simulation and quality evaluation (illustrated as dotted lines in Fig. 4) is executed iteratively by adjusting the variables in the eye image simulator. Consequently, for a given illumination scheme, many sets of quality measurements are created for a range of eye movements and human factors.

The scheme evaluator combines the sets of measurements produced for a range of eye movements and human factors under the same illumination configuration into a single merit function value by computing a weighted sum of squares for the factors being examined. The weights take into account the importance of a given measurement in a particular eye-tracking algorithm, the importance of a corresponding feature for eye tracking, and the accuracy of the feature in a simulated image. The merit function value is used as an accuracy and robustness measurement of the given illumination scheme under different combinations of human factors and angles of eye rotations.

C. Iterative Optimization Process

An approach to optimization would be to first determine an input radiance distribution that yields an illumination for accurate and robust eye tracking out of a database of fictitious input radiance distributions and then create the engineering parameters of source selection and placements that can produce the desired radiance distribution.

In this work, we will detail in Subsection 3.A how we instead characterized an illumination scheme with its irradiance distribution on the incidence plane to simplify the complexity involved in specifying an input radiance distribution starting point to the optimization process. We then utilized the illumination generator to produce the engineering prescription of source configurations for each input distribution. The resulting source model and configurations are then fed into the eye imaging system simulator to create eye images for quality evaluation. The modified optimization loop is formed by the scheme characterizer, illumination generator, system simulator, and image quality evaluation.

The rest of the paper is organized as follows: In Sections 3–5, we detail the implementation of the illumination scheme characterizer, the illumination generator, and the eye imaging system simulator, respectively. In Section 6, we present the results of the simulation of eye illumination in an ET-HMD. Finally, the trade-off of computational efficiency versus accuracy is discussed in Section 7. Detailing the image quality evaluation module and the optimization process is beyond the scope of the paper. Current progress in these modules' development may be found in Pansing [18].

3. Illumination Scheme Characterization

A. Characterizing Input Illumination Schemes

Characterizing a general input radiance distribution requires specifying the intensity magnitude and direction of each ray to be traced, which involves a large parameter space to explore. In the meantime, the optimization framework described in Section 2 requires progressively adjusting the ray magnitudes and directions to produce and evaluate different illumination schemes. The evaluation of each input radiance distribution requires a number of iterations through the eye imaging system and takes a considerable amount of computation time. Therefore, a large parameter space imposes a challenge to a practical implementation in order to yield good accuracy in a reasonable amount of computational time.

To reduce computational complexity, we characterized illumination schemes by their irradiance distribution patterns on the incidence plane when initially determining a good starting point of the input radiance distribution that can yield a good quality of eye illumination. We assumed that radiance distributions with approximately the same magnitude and direction over the eye area will produce similar irradiance distribution patterns on the incidence plane and yield similar quality of eye images. Defining an irradiance distribution on a 2D plane permits a smaller set of parameters than those necessary to characterize complex radiance distributions.

We further approximated the overall irradiance distribution on the incidence plane by the sum of multiple partially overlapping Gaussian distributions. While the number of Gaussian distributions, their spacings, and their fall-off factors may be varied to produce a set of different distributions, different eye-tracking algorithms may impose different constraints. The evaluation of a small set of illumination schemes with considerably different irradiance distributions is required for establishing a good starting point to the optimization.

The optimization process then starts with the established starting point for radiance distribution.

The initial radiance distribution is then perturbed by adjusting its distribution within a reduced range. These perturbed radiance distributions are iteratively evaluated through the same loop of illumination generation, eye image simulation, and image evaluation.

B. Generation of Various Input Irradiance Distributions

In an ET-HMD system, we are particularly interested in the irradiance distribution within an area of 40 mm × 30 mm centered on the cornea vertex to accommodate eye size variations among different user populations [19]. This area further corresponds to the required field of view (FOV) of the eye imaging optics.

By superposing multiple identical Gaussian profiles, a set of irradiance distributions in the incidence plane are created by incrementally varying the peak-offset distance r_i and the fall-off factor δ_i of the ith Gaussian profile. Hereby the peak-offset distance is defined as $r_i = (x_i^2 + y_i^2)^{1/2}$ where (x_i, y_i) is the peak location of the profile on the incidence plane; the fall-off factor is defined as $\delta_i = 1 - \exp(-d^2/8\sigma_i^2)$ where σ_i is the standard deviation of the Gaussian profile and d is the diagonal distance of the eye area of interest.

To create an initial set of testing distributions, we considered four identical Gaussian profiles where the choice for four distributions will be motivated in Subsection 4.A. The peak-offset distance was varied from 0 to 50 mm in 2.5 mm increments. The fall-off factor of the Gaussian profile was varied from 0 (uniform distribution) to 0.95 (sharp drop) in 0.05 increments. This sampling of the parameter space yielded a total of 380 input irradiance distributions, among which 19 distributions have zero peak offset for full overlapping of the Gaussian distributions, varying from uniform illumination to the ones with sharp contrast across the eye area. We compared these samples and selected a subset of visually differing distributions for further investigation. Figure 5 demonstrates a subset of the selected irradiance distributions. It can be observed that as the fall-off factor increases, regardless of the peak-offset distance, the irradiance distributions are highly nonuniform. For a given fall-off factor, the peak-offset distance can be altered to create distributions that demonstrate high uniformity on the incidence plane except a relatively darker center; for instance, the combinations of (0.6, 30) and (0.3, 50). Based on our preliminary evaluation on the eye image quality produced by a variety of distributions [18], we observe that distributions with high fall-off factors produce eye images with high contrast between the pupil and surrounding eye structures, which is in favor of pupil feature segmentation. On the other hand, a uniform distribution produces an image with uniformly illuminated skin area, which is in favor of glint segmentation. Evaluating the simulated images produced by these different distributions will guide the optimal trade-off.

4. Illumination Generator

From all irradiance distributions simulated, a subset of visually differing input irradiance distributions is imported into the illumination generator, where radiance distributions will be simulated and those that are retained produce irradiance patterns on the incidence plane closely matching the inputs. To ensure engineering feasibility, the illumination generator utilizes models of physical illumination sources and takes into account system-specific constraints such as space and source requirements in an ET-HMD system to set up the parametric constraints for the physical source configurations.

A. General Model of Illumination Generator

As illustrated in Fig. 4, the illumination generator consists of creating source models, setting up source parameter space, and applying an optimizer. We assume the usage of IREDs as the physical sources, though other types of sources can be considered as well. Creating source models mainly involves creating the source geometry, source emission profile, and spectral properties. It is desirable to model a collection of sources with different emittance profiles for optimization.

Once source models are selected, the number of sources and the geometrical arrangements (i.e., location and orientation) are the key parameters that affect the radiance distribution created on the incidence plane. The selection of a source number is mainly driven by the requirements of an eye-tracking algorithm as well as the requirement for overall radiant flux. For instance, in many pupil-glint tracking methods, only one glint feature is desired. A common practice is to use one single IRED to create the glint. This approach, however, is usually difficult to yield a good contrast eye image with sufficient robustness. Alternatively, a ring of IREDs may be arranged symmetrically so that their individual glint images are smeared into a symmetrical glint blob for tracking [20]. Another example is the tracking algorithm we proposed recently in our ET-HMD system [15,16], in which we track four individual glints for improved accuracy and robustness. The placement of each IRED is parameterized by its 3D location and its pitch and yaw orientation relative to the XYZ reference.

B. Implementation of Illumination Generator

All the parameters described earlier, including the source model parameters, the number of sources, and source placement parameters, may be theoretically varied to seek for the source configuration that yields the closest match to an input irradiance distribution. However, each system would impose different subsets of variables and constraints. At the early stage of the optimization process, we aimed to vary the footprint of each source on the incidence plane to create an irradiance distribution pattern that matches with an input from the characterizer. Therefore, without loss of generality, we fixed the source model but var-

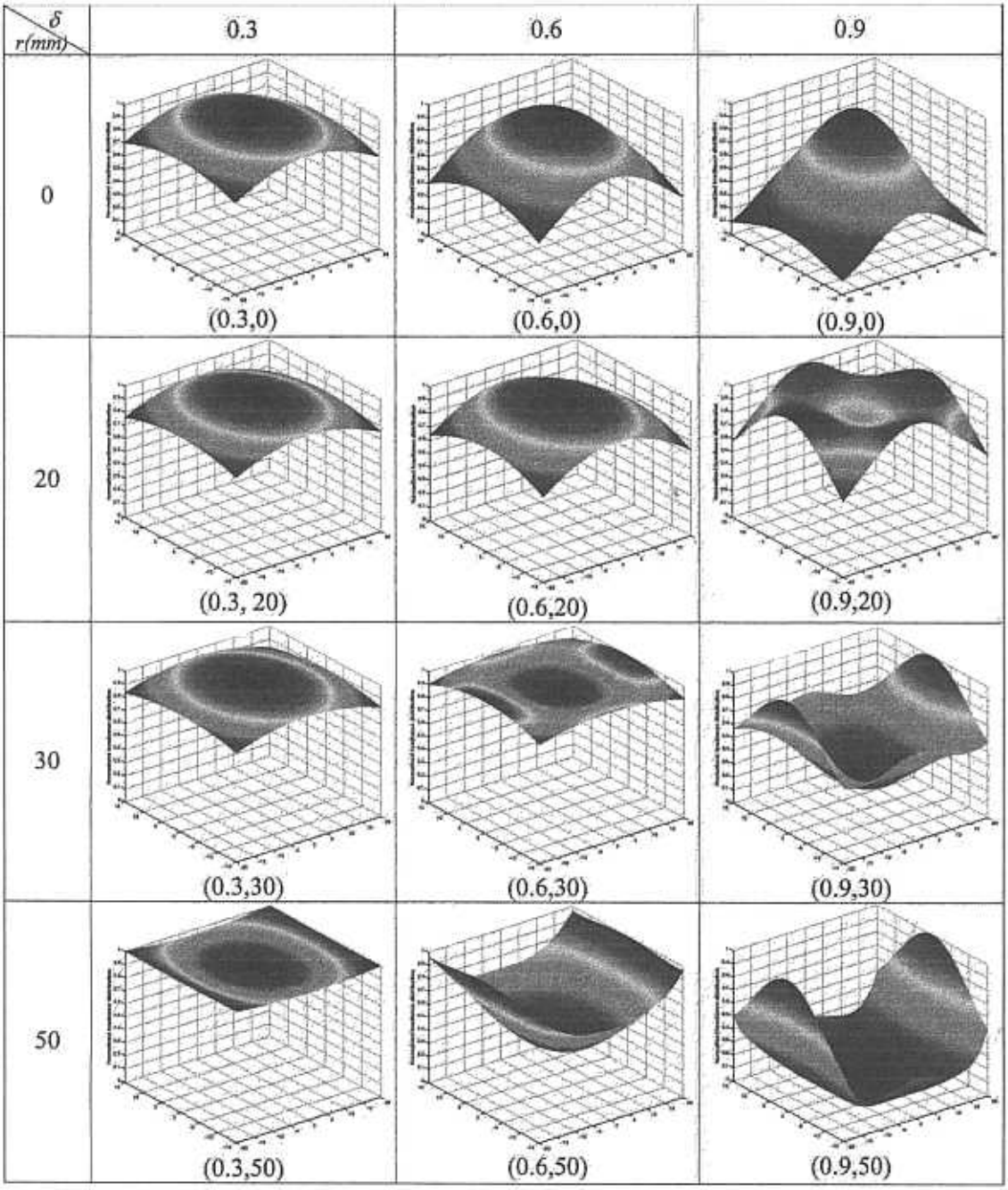

Fig. 5. (Color online) Subset of input irradiance distribution examples using four Gaussian distributions: The peak offset distance r was varied from 0 to 50 mm, and the fall-off factor of the Gaussian profile δ was varied from 0 to 0.95.

ied the geometrical placements of the sources to create the desired footprints. Once an optimal irradiance distribution is established, one may vary both the source model and the placement parameters with constraints inherent to a particular system to create the desired distribution.

The source model we selected is an American Bright IRED source (model number BIR-BO07J4Q-1). This source is rated at a 45° spread angle and an 850 nm wavelength. We modeled this source as a sphere with a 5 mm diameter and the emittance profile set up to approximately match the angular distribution measured from its physical counterpart in our laboratory.

As previously motivated, driven by the requirements of our eye-tracking algorithms [15,16], we fixed the number of IRED sources to be four. Furthermore, to satisfy the geometrical conditions required by the algorithms, we set the four IREDs to be placed on a plane parallel to the incidence plane. These IREDs were placed symmetrically around the optical axis of the imaging system, with one pair of the IREDs placed along the X axis and the other pair along the Y axis. With these constraints, the place-

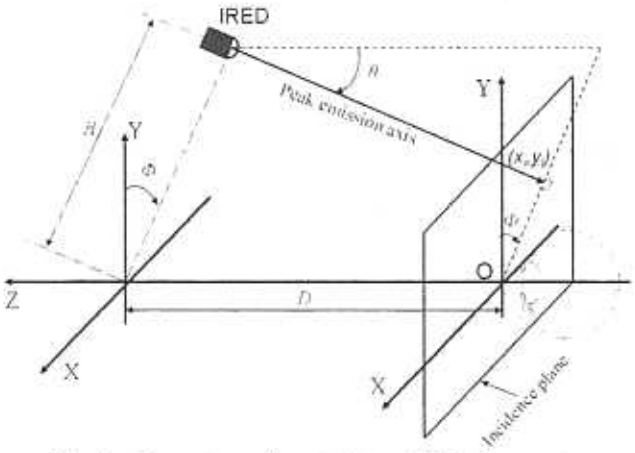

Fig. 6. Parameters characterizing IRED placements.

ment of each IRED was parameterized by two distances and two angles (Fig. 6). The transverse distance, H, offsets laterally the IRED from the optical axis of the eye imaging system. The axial distance, D, offsets the source position from the cornea vertex along the optical axis of the imaging system. This distance affects the area coverage of the individual source and consequently the radiance distribution of each source on the incidence plane. Under the assumption that the IRED axis is always tilted toward the origin of the XYZ reference, the orientation of each source is parameterized by the pitch angle, θ, of its peak emission direction with respect to the optical axis. This angle affects both the offset of the radiance peak and the shape of the irradiance distribution. The polar angle, Φ, characterizes the position of the source relative to the Y axis in the incidence plane. The variable parameters include the transverse and axial distances and the pitch angle that affect the placement of the source relative to the eye.

Driven by the requirements of our eye-tracking algorithms [15,16] in which the geometrical symmetry of the IRED arrangement was utilized to improve tracking accuracy and robustness, the multiple IREDs were arranged symmetrically around a placement circle, for instance, around the aperture of the display optics. Therefore, the transverse distances of the IREDs were set to be identical, equal to the radius of the circle around which the sources were placed. The distance is constrained by the diameter of the optics and the interpupillary distance of the user, thus a range of 20–40 mm was considered. The axial distance of the IREDs is constrained by the eye relief required for an HMD system. We considered ranges from 30 mm, the typical eye relief for immersive HMDs, to 70 mm, eye relief sometimes required for see-through designs. The pitch angle varies from 0°, pointing parallel to the optical axis, to 30°, tipped toward the optical axis.

The simulation tool we selected to use is the LIGHTTOOLS by Optical Research Associates (www.opticalres.com). Currently, the LIGHTTOOLS OPTIMIZER requires the discretization of each parameter. The

Table 1. Summary of Variables for the Illumination Generator

Parameter	Minimum	Maximum	Increment
H (mm)	20	40	2.5
D (mm)	30	70	2.5
θ (degree)	0	30	5

increments for each parameter were selected based on a compromise between the physical setup accuracy and computation time. A summary of the variables, their ranges, and increments are listed in Table 1.

For each possible combination of parameters listed in Table 1, we traced rays from the sources to simulate a unique radiance and corresponding irradiance distribution created on the incidence plane. A 40 mm × 30 mm receiver was set up at the incidence plane facing the sources, which was discretized into 24 × 18 square bins to collect rays from the source and shape the distribution. Each simulated irradiance distribution, corresponding to a specific radiance, was compared against the input irradiances originally generated by the characterizer, and their differences were measured by a root-mean-square (rms) value, the mean and standard deviation of the difference distribution. The optimizer determines the source configuration, and thus the associated radiance distribution, which yields the closest match of the associated irradiance to each of the input irradiances. When compared against the 81 input distributions considered, an analysis shows that the best match is within 2.9% for the normalized mean error.

For each source configuration, tracing a half million rays resulted in a computation time of approximately 10 min to complete the ray trace and determine the merit value against the 81 input irradiances. Thus, finding the source configurations for the 81 input irradiance distributions from the 1071 IRED configurations required approximately 8 days of computation time. It is worth noting that we did not directly use the simulated radiance but the resultant source parameters for simulating eye images, which allows us to trace fewer rays during this step to determine the source parameters rather than millions of rays. The overall computation time was reduced significantly.

5. Eye Imaging System Simulator

The parametric configurations for the IRED sources output by the illumination generator are imported into the eye imaging system simulator to create simulated eye images through an imaging system. Two additional components—the model of eye-facial structures with relevant human factors (e.g., skin color) and an imaging system—are required to complete the eye illumination and image formation process. The eye-facial structures include both the eye optics required for the formation of pupil and glint features and nonoptical elements representing the iris, sclera, and surrounding facial features. Accurately modeling these human tissue structures and

optical properties is important for the evaluation of an illumination scheme under different human factor conditions.

A. Eye Model

The Arizona eye model was adopted for modeling the optical component of the eye structure [21]. While the shape of the eye lens varies when viewing objects at different distances, neglecting it does not affect the accuracy of our analysis, as we will use only the reflection by the anterior corneal surface for glint formation and the refraction of the corneal surfaces for pupil/iris imaging.

The eye optics were integrated into a spherical eyeball structure with a 28 mm diameter [22]. Considering the typically reduced illumination levels in HMDs, we assumed a 4 mm pupil in the simulation. The outer boundary of the iris with the sclera often imposes the limit on which glints can be detected robustly. Based on anthropometric measurements [19], the diameter of the iris's outer boundary was set to be 11.5 mm. To simulate the effects of eye rotation on image quality, the entire eyeball structure was set to be rotationally symmetric and to pivot around a center of rotation located 15 mm behind the cornea vertex [23]. The angles of eye rotation were investigated as variables in the optimization process.

Although secondary reflection images, besides the first Purkinje image, could be formed through the surfaces of the posterior cornea and the eye lens, they are sufficiently dim and do not interfere with the detection of the glints in our eye-tracking system due to the low Fresnel reflectance of these surfaces and the usage of low power IRED sources [15,16]. Therefore, all the refractive elements in the eye optics were set to 100% transmittance, except the anterior cornea, which was assigned a 97.6% transmittance and a 2.4% specular reflectance approximated with the Fresnel reflectance equation at normal incidence. The 2.4% reflectance of the anterior cornea contributes to the formation of glints. Little information on spectral data for the sclera was identified in the literature. Therefore, to estimate the diffuse reflectance, the average irradiance value of the sclera feature was estimated from real eye images taken under relative uniform illumination. The average values were further normalized to the accepted Caucasian skin reflectance, which will be discussed in Subsection 5.B. As a result, the sclera has been modeled with 45% diffuse reflectance. The specular reflectance of the sclera has been set to 2% using the Fresnel reflectance for a tear layer with a refractive index of 1.34 [24]. The refractive index of the iris was not identified in the literature and thus was assumed to be close enough to the aqueous humor index. Consequently, the specular reflectance of the iris was assumed to be negligible based on Fresnel reflectance. The diffuse reflectance of the iris, however, is expected to vary with iris color, and thus is one of the human factors to be investigated in the optimization process. Due to the lack of literature evidence, the diffuse reflectance of the iris was estimated using the same approach that we used to estimate the diffuse reflectance for the sclera. Based on estimates from real images and normalization to the skin reflectance, a blue iris was estimated to have a 25% diffuse reflectance.

Finally, other factors such as contact lenses, glasses, and even eyes that had LASIK surgery can be modeled and investigated similarly to other human factors for their effects on eye image quality and tracking robustness. The investigation of these factors is beyond the scope of the current study.

B. Facial Feature and Skin Modeling

Although facial features surrounding the eyeball, such as the cheek, eyebrow, and nose, are not the key features of interest in an eye-tracking system in general, some of these features are often present in an eye image, since an FOV slightly larger than the eyeball is required to accommodate eye size variations and possible helmet slippage. Improper illumination of these features can impose difficulty in pupil and glint segmentation (Fig. 3). The illumination levels of these features should be simulated for image quality assessment.

The geometries of these features usually vary from person to person and should be considered as one of the human factors. It is, however, unrealistic to evaluate each illumination scheme on millions of faces. Furthermore, the subtle variations of facial geometry will mainly affect the local uniformity in simulated eye images, rather than the average skin irradiance. For threshold-based feature segmentation algorithms, local nonuniformity of the facial features can be tolerated if high contrast between the facial and eye features are warranted. Therefore, we used a laser scan data set obtained from a real patient to model the geometry of the facial structures. The data set was provided by a 3D human model available from Zygote and e-Frontier (www.open3dproject.org).

While many unique models of varying complexity have been developed to characterize the optical properties of human tissue, most notably for human skin simulation in medical and computer graphics applications [25], our interest is in the cumulative superficial properties. Therefore, the spectral data of these

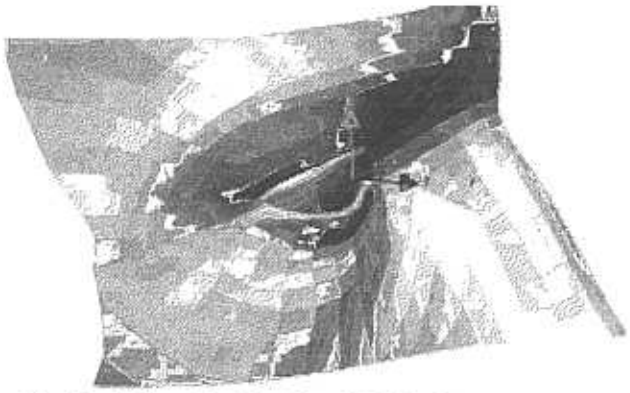

Fig. 7. (Color online) Combined facial and eye structures.

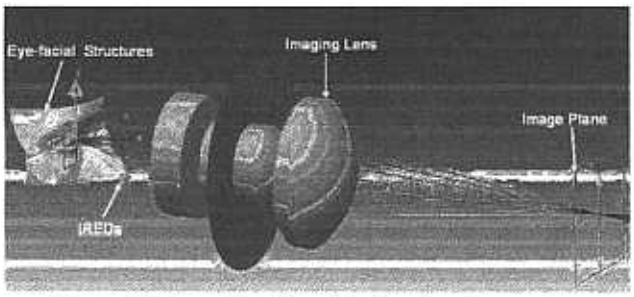

Fig. 8. (Color online) Simulated eye imaging system.

facial features was modeled by a computationally simple method that combines the diffuse and specular properties of many skin layers—the stratum corneum, epidermis, and dermis—into one layer. The primary contributor to the skin diffuse component is the dermis, and medical literature has reported the skin diffuse reflectance to be 60% in the near infrared (NIR) for Caucasian skin and 45% for black skin [26,27]. The primary specular component, however, is at the boundary between the air and the stratum corneum, which has a refractive index of 1.55 [28]. A specular reflectance of 5% was estimated with a Fresnel reflectance equation at normal incidence. To simulate the effects of skin color on eye image quality, the skin diffuse reflectance is considered as one of the human factors to be investigated in the optimization process. The integration of the facial structure and the eye model is shown in Fig. 7 with an eye area of 40 mm × 30 mm as the primary region of interest.

C. Combined Illumination and Eye Imaging Simulation

The combined model of the eye illumination and imaging simulation is shown in Fig. 8. Rays originating from the IREDs scatter off the eye structure. As our goal is to simulate the eye illumination-imaging process, without loss of generality, an imaging optics with a large aperture was chosen to efficiently collect the scattered rays off the eye model and focus them onto a receiver located at the image plane [29]. In the simulation, the image receiver was divided into 87 × 65 bins to form a simulated eye image of reasonable quality and computation time. Simulating an eye image through the system by tracing 3.5×10^6 rays takes ~2 h on a Pentium 4 3.2 GHz machine with 1 GByte of memory.

6. Simulation Results

To illustrate the overall modeling framework, we selected two examples from the 81 irradiance distributions generated in Subsection 3.B. In both examples, each Gaussian profile had a fall-off factor of 0.8. However, the peak-offset distance of each fictitious source from the center was zero in the first scheme with a 20 mm offset in the second scheme. Consequently, the first scheme physically corresponds to an irradiance distribution in a Gaussian pattern over the incidence plan, while the second one represents a relatively uniform distribution in the center area with a slow drop close to the edge. The simulated irradiances for these two schemes are shown in Figs. 9(a) and 9(d), respectively. A series of simulated eye images under these two schemes are also shown in

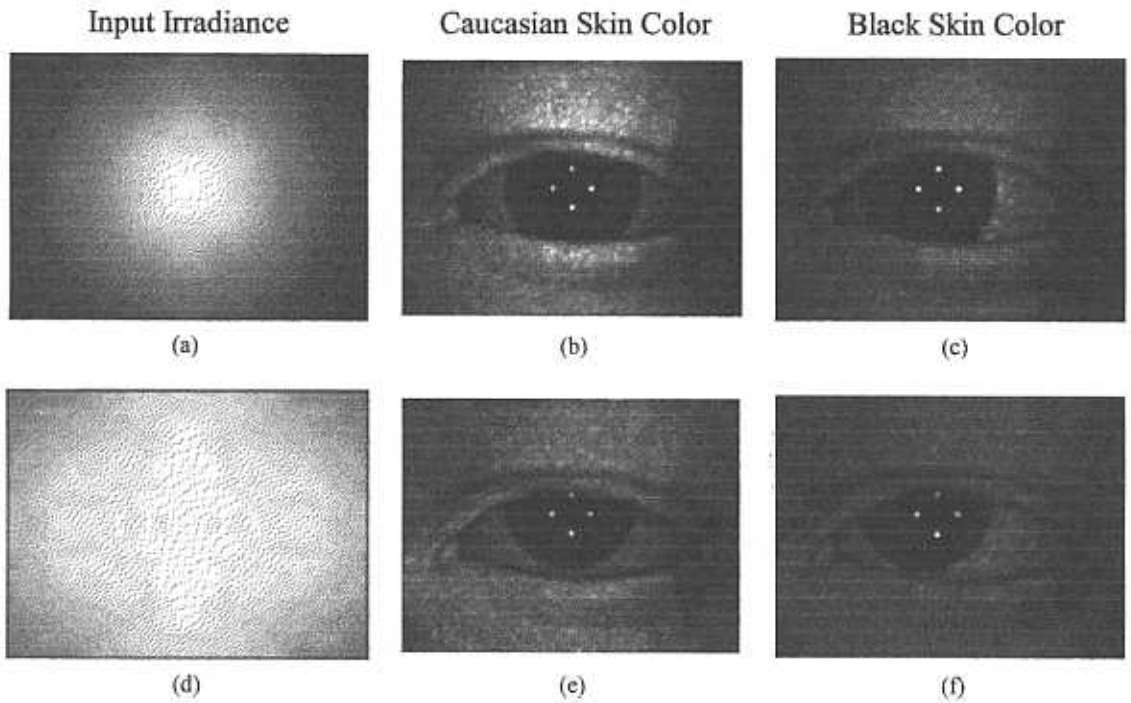

Fig. 9. Example of simulated results: (a) Simulated input irradiance with δ equal to 0.8 and r equal to 0 mm; (b), (c) simulated eye images from input irradiance in (a), for (b) zero eye rotation along with Caucasian skin, and (c) 10° horizontal eye rotation combined with black skin; (d) simulated input irradiance with δ equal to 0.8 and r equal to 20 mm; (e), (f) simulated eye images from input irradiance in (d), for (e) 10° vertical eye rotation along with Caucasian skin, and (f) 10° diagonal eye rotation combined with black skin.

Fig. 9 under different combinations of eye rotation angles and skin color. Figure 9(b) shows a simulated image when no eye rotation is applied to the system, while Figs. 9(c), 9(e), and 9(f) are computed with a 10° eye rotation in the horizontal, vertical, and diagonal directions, respectively. The center and right columns demonstrate the boundary range of skin colors applied in the system: the center column [Figs. 9(b) and 9(e)] is the upper reflectance boundary associated with Caucasian skin (reflectance equal to 60%); and the right column [Figs. 9(c) and 9(f)] is the lower reflectance boundary that represents black skin (reflectance equal to 45%). Important features in the simulated images correlate well with the necessary features present in actual eye images. The glint positions and pupil boundary are accurately recreated, as are the other features of the eye structure.

Under identical illumination schemes, a numerical comparison of skin irradiance values was performed pixel by pixel between the middle and right columns of the simulated eye images. Results showed that the ratio of the skin irradiance values of the images simulated with the black skin and the Caucasian skin is 77% on average, which matches the ratio of the skin reflectance coefficients. Under the Caucasian skin condition, further analysis was performed on the images created by the two different illumination schemes (top and bottom rows) to estimate the average irradiance and nonuniformity of the skin and its contrast to the pupil. The first input illumination (top row) resulted in an average contrast of 35% between the skin and pupil, while the second input illumination (bottom row) had an average contrast of 49%. The nonuniformity of the average skin area was 21% for the Gaussian input, and 19% for the second input irradiance. The second illumination scheme is better than the first one as it potentially allows an easier and more accurate segmentation of the pupil feature from the skin. While it is beyond the scope of this paper to further detail the metrics for image quality assessment, rigorous metrics are being developed to quantify the quality of these images for tracking [18].

By turning on and off the reflectance of relevant features in the eye-facial model, the simulated model can be conveniently controlled to generate a set of mask images that are used to facilitate the segmentation of the features of interest. Figures 10(b)–10(d) show the segmentation of the skin area, the entire eyeball, and the sclera region, respectively, for the image provided in Fig. 10(a). These mask images are applied to a simulated eye image in order to segment the key features critical to an eye-tracking algorithm. The module of image quality evaluation will then compute the brightness, uniformity, and contrast of these features and these measurements are used to form a quality metric for an individual image by the quality evaluator (Fig. 4). Under a given illumination scheme, the quality evaluator is iteratively executed on a set of simulated images generated under a range of eye rotation angles and human factors in the eye model. The resultant quality measurements for these images are imported to the scheme evaluator, which

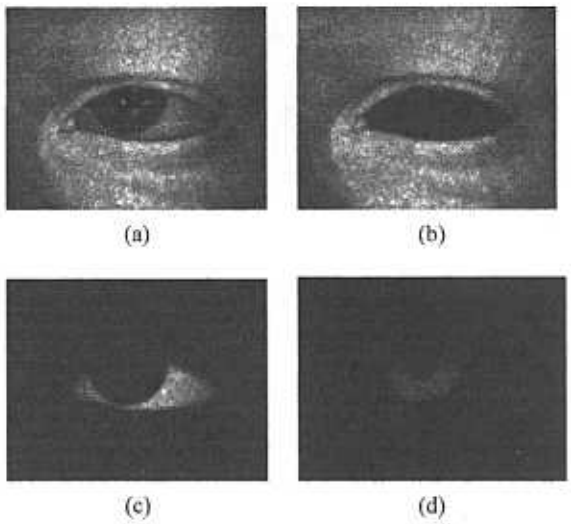

Fig. 10. Example of mask generation: (a) Simulated eye image; (b) masked image revealing the skin area; (c) masked image revealing the sclera; (d) masked image revealing the iris-pupil area with glints removed.

generates a single merit value of the given illumination. The single merit value is a weighted measurement that takes into account factors such as eye rotation range, the importance of an eye feature in a given tracking algorithm, and the accuracy of each eye feature. For instance, the quality measurements of the images corresponding to a central range of eye movements are weighted more in the merit value than those of large eye movements. Preliminary results on the development of quality evaluation procedures may be found in [18].

7. Ray-Tracing Speed versus Accuracy

The model described earlier provides us with the capability of simulating resultant eye images with a combination of illumination schemes and human factors. A key concern in any illumination model is the minimal number of rays to be traced, which offers the ability to create images with adequate accuracy for quality evaluation. Applying the Rose model summarized in Subsection 7.A [30], we examine the trade off between ray-tracing speed and accuracy in Subsection 7.B.

A. Rose Model

A statistical model was developed for cameras operating at low-light levels where the random distribution of arriving photons sets a limit on the achievable image quality [30]. The model elegantly relates image resolution, contrast, and signal-to-noise ratio (SNR) to the number of photons incident upon a detector. The low-light level imaging situation is analogous to the simulation of an illumination system where a limited number of rays in a random distribution are traced. Recently the Rose model has been applied to the analysis of illumination systems [31,32].

Derived from the Rose model, in order to resolve a minimal feature of area A in a background of area A_o,

the minimum number of rays required to be incident on the feature is given by

$$M_{\min} = \frac{A_o}{A} \frac{k^2}{C^2}, \tag{1}$$

where C is the minimal contrast between a resolvable feature and background and k is the desired SNR. The minimal feature contrast is the relative irradiance difference between the feature of interest and the background and is defined as

$$C = \frac{\Delta E}{E}, \tag{2}$$

where E is the background irradiance and ΔE is the irradiance difference between the local background and a feature. As expected, the Rose model points to the need to trace more rays in order to resolve small-size, low-contrast features but also provides quantitative guidelines.

The random nature of ray-trace distributions causes fluctuations in the simulated irradiance at the image plane and these fluctuations may be mistakenly recognized as a feature of interest, or conversely a real feature may become irresolvable from the background. Consider a bright feature. To discern the feature unambiguously, the feature's irradiance must be larger than the statistical fluctuations of the background irradiance that are usually modeled with a normal distribution. Let σ be the standard deviation of the background fluctuations within areas of size A set by the feature size and let $P_N(k\sigma)$ denote the probability in which an illumination fluctuation is larger than $k\sigma$ within areas A. Hereby the desired SNR, k, measures the allowable fluctuations in a simulated illumination distribution. If the irradiance difference of the feature satisfies $\Delta E \geq k\sigma$, then the probability of obtaining a false feature with areas of size A within the background area A_o, P_{false}, is given by

$$P_{false} = 2 \frac{A_o}{A} P_N(k\sigma), \tag{3}$$

where a factor of 2 accounts for the possibility of having a fluctuation either larger or smaller than the average E. Once a user sets the desired probability of false features, the desired SNR, k, can be found by interpolating from the $P_N(k\sigma)$ for a normal distribution. The minimal number of rays received by the image plane can then be calculated using Eq. (1).

B. Application of the Rose Model

The Rose model can be utilized to determine the minimal number of rays to be collected by the image plane in a simulated imaging system in order to resolve a certain feature of interest. In our application, the image plane is divided into S by T pixels (e.g., currently 87 × 65 pixels) and we apply the Rose model to determine the number of rays needed to be collected by each pixel to obtain a given level of pixel accuracy. Therefore, both the minimal resolvable feature area and the background area are set to be 1 pixel, which leads to $A_o/A = 1$ in Eqs. (1) and (3). To achieve a given level of pixel accuracy, the minimum number of rays to be traced through the system for the entire image plane is

$$M_{\min} = \frac{STk^2}{eC^2}, \tag{4}$$

where e is the transfer efficiency of an illumination system from its source to the image plane.

Table 2. Minimally Traced Rays and Computation Time Vary with Desired Pixel Accuracy and Feature Contrast[a]

P_{false}	Contrast	Rays/Pixel	Total Traced Rays (10^6)	Estimated Time (hr)
1%	0.05	2,704	46	26
	0.1	676	11	7
	0.2	169	2.9	2
5%	0.05	1,444	24	14
	0.1	361	6.1	3
	0.2	90	1.5	1
10%	0.05	784	13	8
	0.1	196	3.3	2
	0.2	49	0.83	<1

[a]Assumption: 87 × 65 pixels and 33% transfer efficiency.

Using different combinations of pixel accuracy and minimal feature accuracy, Table 2 summarizes the minimal number of rays collected by each pixel and traced through the system as well as the estimates of computation time, under the assumptions of an image resolution of 87 × 65 pixels and an optical transfer efficiency of 33%, which is the approximate efficiency of the simulated illumination-imaging system described in Section 5. The computation time estimation was based on a Pentium IV desktop with a 3.2 GHz CPU and 1 GByte of memory.

In the examples previously shown in Fig. 9, 3.5 × 10^6 rays were traced for each eye image. Analysis has shown that an average ray density typically ranges from 150 to 200 rays/pixel, which falls in the range estimated by the Rose model. The results indicate that the pixels of the simulated images have ~90% accuracy for features with a contrast of at least 10%, and ~99% of accuracy for features with a contrast greater than 20%. Therefore, it is expected that in these simulated images brighter eye-facial features have a higher accuracy than the relatively darker features such as irises.

8. Conclusion

In this paper, we detail a framework to optimize illumination schemes within an ET-HMD. The overall goal is to identify illumination schemes that are optimized for pupil-corneal based eye-tracking applications, which are tolerant of various human factors and eye rotations, and therefore more capable of ef-

ficient and robust eye tracking. In this specific paper, we detailed the system modeling module employed to generate user-defined illumination schemes and to simulate the light interaction between a prescribed illumination scheme and the eye structure. We further analyzed the relationship between ray-tracing speed and accuracy by applying the Rose model. The simulation described in this paper provides the capability of simulating resultant eye images for a variety of illumination schemes. Future research will report on the development of a set of measurements for selected eye-tracking algorithms to quantify the quality of eye images created under different combinations of illumination schemes, angles of eye rotation, and human factor variations.

This research is supported by the National Science Foundation grants IIS-03-07227/04-11578 and 03-07189. We acknowledge Kevin Tompson from Optical Research Associates and John Koshel from Lambda Research Corporation for stimulating discussions.

References

1. W. Barfield and T. Caudell, eds., *Fundamentals of Wearable Computers and Augmented Reality* (Lawrence Erlbaum Associates, 2001).
2. O. Bimber and R. Raskar, *Spatial Augmented Reality: Merging Real and Virtual Worlds* (A. K. Peters, 2005).
3. O. Cakmakci and J. P. Rolland, "Head-worn displays: a review," J. Display Technol. **2,** 199–216 (2006).
4. R. J. K. Jacob and K. S. Karn, "Eye tracking in human-computer interaction and usability research: ready to deliver the promises (Section Commentary)," in *The Mind's Eye: Cognitive and Applied Aspects of Eye Movement Research,* J. Hyona, R. Radach, and H. Deubel, eds. (Elsevier Science, 2003), pp. 573–605.
5. M. Hayhoe, D. Ballard, J. Triesch, and H. Shinoda, "Vision in natural and virtual environments," in *Proceedings of ACM 2002 Symposium of Eye Tracking Research and Applications* (ACM, 2002), pp. 7–13.
6. J. Rolland, Y. Ha, and C. Fidopiastis, "Albertian errors in head-mounted displays: I. Choice of eye-point location for a near- or far-field task visualization," J. Opt. Soc. Am. A **21,** 901–912 (2004).
7. K. Iwamoto, K. Komoriya, and K. Tanie, "Eye movement tracking type image display system for wide view image presentation with high-resolution: evaluation of high-resolution image presentation," in *International Conference on Intelligent Robots and Systems* (IEEE, 2002), pp. 1190–1195.
8. A. T. Duchowski, "Incorporating the viewer's point-of-regard (POR) in gaze-contingent virtual environments," Proc. SPIE **3295,** 332–343 (1998).
9. L. Vaissie and J. Rolland, "Head mounted display with eye tracking capability," U.S. patent 6,433,760 (13 August 2002).
10. H. Hua, "Integration of eye tracking capability into optical see-through head mounted displays," Proc. SPIE **4297,** 496–503 (2001).
11. C. Curatu, H. Hua, and J. Rolland, "Projection-based head mounted display with eye tracking capabilities," Proc. SPIE **5875,** 128–140 (2005).
12. A. T. Duchowski, *Eye Tracking Methodology: Theory and Practice* (Springer-Verlag, 2003).
13. M. Eizenman, R. C. Frecker, and P. E. Hallett, "Precise non-contacting measurement of eye movements using the corneal reflex," Vision Res. **24,** 167–174 (1984).
14. T. N. Cornsweet and H. D. Crane, "Accurate two-dimensional eye tracker using first and fourth Purkinje images," J. Opt. Soc. Am. **63,** 921–928 (1973).
15. H. Hua, P. Krishnaswamy, and J. P. Rolland, "Video-based eyetracking methods and algorithms in head-mounted displays," Opt. Express **14,** 4328–4350 (2006).
16. P. Krishnaswamy, "Design and assessment of improved feature-based eye tracking methods for head-mounted displays," M.S. thesis (Department of Electrical and Computer Engineering, University of Arizona, 2005).
17. C. W. Pansing, H. Hua, and J. P. Rolland, "Optimization of illumination schemes in a head-mounted display integrated with eye tracking capabilities," Proc. SPIE **5875,** 587501 (2005).
18. C. Pansing, "Optimization of illumination schemes for an eye-tracked head mounted display," M.S. thesis (College of Optical Sciences, University of Arizona, 2006).
19. L. G. Farkas, *Anthropometry of the Head and Face,* 2nd ed. (Raven, 1994).
20. C. H. Morimoto, D. Koons, A. Amir, and M. Flickner, "Pupil detection and tracking using multiple light sources," Image Vision Comput. **18,** 331–335 (2000).
21. J. Schwiegerling, *Field Guide to Visual and Opthalmic Optics* (SPIE, 2004).
22. T. W. Olsen, S. Y. Aaberg, D. H. Geroski, and H. F. Edelhauser, "Human sclera: thickness and surface area," Am. J. Opthamol. **125,** 237–241 (1998).
23. D. A. Atchison and G. Smith, *Optics of the Human Eye* (Reed Educational and Professional, 2000).
24. J. P. Craig, P. A. Simmons, S. Patel, and A. Tomlinson, "Refractive index and osmolality of human tears," Optom. Vision Sci. **72,** 718–724 (1995).
25. G. V. G. Baranoski and A. Krishnaswamy, "An introduction to light interaction with human skin," RITA **9,** 33–62 (2004).
26. R. R. Anderson, J. Hu, and J. A. Parrish, "Optical radiation transfer in the human skin and applications in vivo remittance spectroscopy," in *Bioengineering and the Skin,* R. Marks and P. A. Payne, eds. (MTP Press Ltd., 1981).
27. G. Wyszecki and W. S. Stiles, *Color Science: Concepts and Methods, Quantitative Data and Formulae* (Wiley, 1982).
28. V. Tuchin, *Tissue Optics* (SPIE, 2000).
29. J. G. Baker, "Highly corrected objective having two inner divergent meniscus components between collective components," U.S. patent 2,532,751 (5 December 1950).
30. A. Rose, *Vision: Human and Electronic* (Kluwer Academic, 1973).
31. R. J. Koshel, "Aspects of illumination system optimization," Proc. SPIE **5529,** 206–217 (2004).
32. G. L. Perterson, "How many rays do I need to trace? Applying the Rose model to computer analysis of illumination systems," Breault Research Organization White Paper (3 January 2005).